EPJ manuscript No.
(will be inserted by the editor)

Open and Hidden Charm Production in dA Collisions at RHIC and LHC

R. Vogt

[1] Lawrence Berkeley National Laboratory, Berkeley, CA 94720, USA
[2] Physics Department, University of California, Davis, CA 95616, USA

Received: date / Revised version: date

Abstract. We discuss aspects of open and hidden charm production in deuterium-nucleus collisions at RHIC and LHC energies. We describe calculations of the total $c\overline{c}$ cross section and the charm quark transverse momentum distributions. We next explain how shadowing and moderate nuclear absorption can explain the PHENIX J/ψ dAu/pp ratios and predict the combined effect of shadowing and absorption in 6.2 TeV d+Pb collisions.

1 Introduction

Heavy flavors were one of the first true hard probes of heavy ion collisions through the J/ψ measurements of NA38 and its successors [1]. These measurements also showed the importance of baseline measurements in pp and pA interactions to separate 'normal' from 'anomalous' behavior. Now, after initial Au+Au runs at RHIC, the first baseline pp and d+Au heavy flavor data have been reported, both open charm and J/ψ, "hidden" charm.

Leptons originating from open charm decays were separated for the first time in a heavy ion environment by PHENIX in Au+Au collisions at $\sqrt{S_{NN}} = 130$ GeV [2]. Now STAR has results both in the lepton channel [3] and in the spectra of reconstructed D mesons [4]. These measurements will help more fully understand open charm production in AA collisions where energy loss [5], flow [6] and regeneration of J/ψ by $c\overline{c}$ [7] may be important. The J/ψ, on the other hand, while well measured at the SPS, awaits data from the 2004 Au+Au run to provide a higher statistics measurement of J/ψ production at 200 GeV. The d+Au J/ψ data, over a wide rapidity range, provide interesting hints of the behavior of the nuclear gluon distribution. We discuss our dA calculations at RHIC and provide predictions for J/ψ production in d+Pb collisions at the LHC.

2 Open Charm

Open charm measurements date back to the late 1970s when D and $\overline{D}$ mesons were first detected, completing the picture of the fourth quark begun when the J/ψ was detected in pBe and e^+e^- interactions. The charm quark was postulated to have a mass between 1.2 and 1.8 GeV. Because of its relatively large mass, it is possible to calculate a total $c\overline{c}$ cross section using perturbative quantum chromodynamics (pQCD), not the case for lighter flavors. Charm hadrons are usually detected two ways. The reconstruction of charged hadron decays such as $D^0 \to K^-\pi^+$ (3.8%) and $D^+ \to K^-\pi^+\pi^+$ (9.1%) gives the full momentum of the initial D meson, yielding the best direct measurement. Charm can also be detected indirectly via semi-leptonic decays such as $D \to Kl\nu_l$ although the momentum of the parent D meson remains unknown. Early measurements of prompt leptons in beam dump experiments assumed that the density of the dump was high enough to absorb semi-leptonic decays of non-charm hadrons, leaving only the charm component. At modern colliders, it is not possible to use beam dumps to measure charm from leptons but, at sufficiently high p_T, electrons from charm emerge from hadronic cocktails [3,8].

Extracting the total charm cross section is a non-trivial task. To go from a finite number of measured D mesons in a particular decay channel to the total $c\overline{c}$ cross section one must: divide by the branching ratio; correct for the luminosity, $\sigma_D = N_D/\mathcal{L}t$; extrapolate to full phase space from the finite detector acceptance; divide by two to get the pair cross section from the single Ds; and multiply by a correction factor [9] to account for the unmeasured charm hadrons, primarily D_s and Λ_c. There are assumptions all along the way. The most important is the extrapolation to full phase space. Before QCD calculations were available, the data were extrapolated assuming a power law for the x_F distribution, related to the longitudinal momentum of the charm hadron by $x_F = p_z/(\sqrt{S}/2) = 2m_T \sinh y/\sqrt{S}$. The canonical parameterization for extrapolation over all x_F is $(1-x_F)^c$ where c was either fit to data over a finite x_F range or simply assumed. These parameterizations could lead to large overestimates of the total cross section if $0 < c < 2$ was assumed, especially when data were taken only near $x_F = 0$. Lepton measurements, particularly using beam dumps, resulted in more conservative cross sections but were typically at more forward x_F.

2.1 Total cross section

There has been a great deal of improvement over the last 10-15 years. Next-to-leading order (NLO) calculations are used in the phase space extrapolation, resulting in considerably less ambiguity in the shape of the x_F distributions, $d\sigma/dx_F$. The transverse momentum distributions are more difficult, as we will discuss later. To calculate the total cross section to NLO, scaling functions [10] proportional to logs of μ^2/m^2 are useful where μ is the scale of the hard process. The hadronic cross section in pp collisions can be written as

$$\sigma_{pp}(S,m^2) = \sum_{i,j} \int dx_1\, dx_2\, f_i^p(x_1,\mu_F^2)\, f_j^p(x_2,\mu_F^2)\, \widehat{\sigma}_{ij}(s,m^2,\mu_F^2,\mu_R^2) \quad (1)$$

where the sum over i,j runs over q, $\overline{q}$ and g while x_1 and x_2 are the fractional momenta carried by the colliding partons and f_i^p are the proton parton densities. The partonic cross sections are

$$\widehat{\sigma}_{ij}(s,m,\mu_F^2,\mu_R^2) = \frac{\alpha_s^2(\mu_R^2)}{m^2}\left\{ f_{ij}^{(0,0)}(\rho) + 4\pi\alpha_s(\mu_R^2)\left[f_{ij}^{(1,0)}(\rho) + f_{ij}^{(1,1)}(\rho)\ln\left(\frac{\mu_F^2}{m^2}\right)\right] + \mathcal{O}(\alpha_s^2)\right\} \quad (2)$$

with s the squared partonic center of mass energy, $\rho = 4m^2/s$ and $f_{ij}^{(k,l)}$ are the scaling functions given to NLO in Ref. [10]. It is most consistent to assume that the factorization scale, μ_F, and the renormalization scale, μ_R, are equal, $\mu = \mu_F = \mu_R$ although this may underestimate the theoretical uncertainties. There is no dependence on the kinematic variables. Some NNLO calculations are available near threshold, $s = x_1 x_2 S \sim 1.3\,(4m^2)$, applicable only for $\sqrt{S} \leq 20-25$ GeV [11,12]. The NLO corrections to the leading order (LO) cross sections are relatively large, $K^{(1)} = \sigma_{\rm NLO}/\sigma_{\rm LO} \sim 2-3$, depending on μ, m and the parton densities [13].

The approximate NNLO corrections, obtained through a re-expansion of the threshold-resummed cross section to $\mathcal{O}(\alpha_s^4)$, are about as large to next-to-next-to-leading logarithm [11] but decrease to less than $K^{(1)}$ when subleading logs are included [12]. This K factor is large because, in the range $1.2 < m < 1.8$ GeV, $m < \mu < 2m$ with a 5-flavor QCD scale, Λ_5, of 0.153 GeV for the GRV98 HO and 0.22 GeV for the MRST parton densities, giving $0.21 < \alpha_s(c) < 0.4$.

Instead of presenting a wide range of possible cross sections and emphasizing the uncertainties, the approach taken in Ref. [14] has been to "fit" m and μ for a particular parton density and extrapolate to higher energies. The results are compared to some of the total cross section data [9] on the left-hand side of Fig. 1. The data tend to favor lower values of m, $1.2-1.3$ GeV. The two curves cross each other because the MRST calculation with $\mu = 2m$ increases faster at large $\sqrt{S}$ and smaller x due to the stronger QCD evolution of the parton densities at the higher scale. Although the fixed target results are in good agreement with the calculations, the PHENIX point [2] at 130 GeV, from Au+Au electron measurements, and the STAR point [15], from a combination of electron and reconstructed D measurements, are generally above the calculations. The STAR point is about a factor of four over the calculated cross section. The higher energy $p\overline{p}$ data from UA1 [16] and CDF [17] (not shown, the CDF data are, in any case, only at high p_T, not allowing a total cross section measurement) are in better agreement with the calculations.

2.2 Transverse momentum distributions

Now we turn to the transverse momentum, p_T, distributions. In this case, the quark mass is no longer the only scale and p_T-dependent logs also appear. Thus, to interpolate between the high p_T scale set by p_T and the low p_T mass scale, a scale μ proportional to m_T, the transverse mass, is the natural choice. The charm quark p_T distributions are not strongly dependent on quark mass for $p_T \geq 3$ GeV, as may be expected, where the difference in rate is $\approx 20\%$ between $m = 1.2$ and 1.8 GeV. The difference in the total cross sections is almost all at $p_T \leq 3$ GeV. Changing the scale changes the slope of the p_T distributions. The distributions are harder for $\mu = m$ than $\mu = 2m$. The average p_T, $\langle p_T \rangle$, increases with m and is larger for $\mu = m$.

It is not enough to equate the charm quark and the D meson since hadronization, $c \to D$, may involve some momentum loss by the quark. If factorization holds in the final state (universal fragmentation functions) as well as in the initial state (universal parton distributions) then the fragmentation functions extracted in e^+e^- should also be applicable to pp and dA. However, this assumption typically does not work well for charm [18]. The Peterson fragmentation function [19], typically used in hadroproduction codes, is parameterized as

$$D_{c/H}(z) = N\frac{1}{z}\left(1 - \frac{1}{z} - \frac{\epsilon_c}{1-z}\right)^{-2} \quad (3)$$

where $\epsilon_c = 0.06$ was fit to pre-LEP e^+e^- data [20], reducing the charm hadron momentum by 30% relative to the charm quark. Current measurements by Belle give a slightly smaller value of $\epsilon_c = 0.052$ and also suggest that this functional form gives the worst fit to the data of all the fragmentation functions compared to the data [21]. Fragmentation functions calculated in Mellin moment, n, space instead of z space, such as the Peterson function, tend to predict lower momentum loss by the heavy quark, reducing ϵ_c by up to an order of magnitude in the z-space representation [22]. (In low $\sqrt{S}$ collisions, the momentum reduction due to fragmentation can be compensated by intrinsic transverse momentum, k_T, broadening. However, such broadening cannot compensate the x_F distributions, only marginally affected by k_T smearing. We have previously shown that the D meson x_F distributions are consistent with no momentum loss during charm quark hadronization [18].) The exclusive NLO $Q\overline{Q}$ code

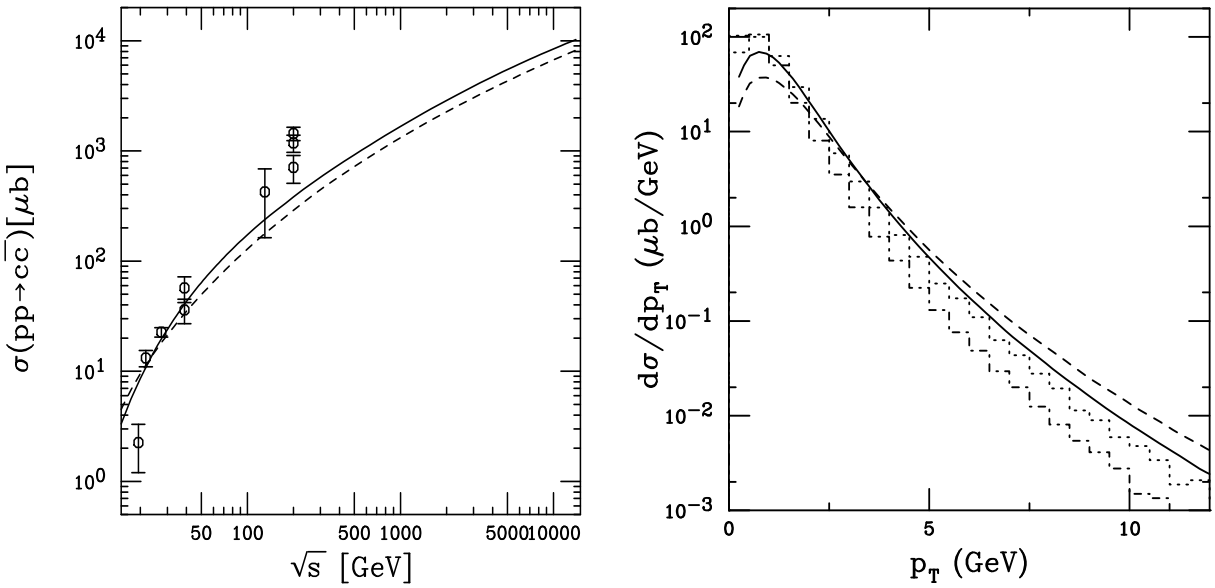

Fig. 1. The NLO total $c\bar{c}$ cross sections as a function of $\sqrt{S}$ (left-hand side) and charm quark p_T distribution at $\sqrt{S} = 200$ GeV in the range $|y| \leq 1$ (right-hand side) in pp interactions. The curves are MRST HO (solid) with $m = 1.2$ GeV and $\mu^2 = 4m^2$ and GRV98 HO (dashed) with $m = 1.3$ GeV and $\mu^2 = m^2$. The two histograms include fragmentation with the Peterson function using $\epsilon_c = 0.06$ (dot-dashed) and 0.006 (dotted).

of Ref. [23] includes Peterson fragmentation and intrinsic transverse momentum, k_T, broadening by adding the k_T kick in the final, rather than the initial state.

The effects of fragmentation and intrinsic k_T broadening of $\langle k_T^2 \rangle = 1$ GeV^2 compensate each other at $\sqrt{S} = 20$ GeV to give a D meson p_T distribution very similar to that of the charm quark. This outcome is desirable because the D p_T and x_F distributions are similar to those of the charm quark at fixed-target energies [18]. However, at RHIC energies, due to the higher $\langle p_T \rangle$ at larger $\sqrt{S}$, the effect of broadening is relatively small and cannot compensate for the momentum loss induced by fragmentation. Interestingly enough, the STAR D and D^* p_T distribution also agrees rather well with the NLO charm quark distribution [4]. On the right-hand side of Fig. 1, we show the p_T distributions at $\sqrt{S} = 200$ GeV for the two sets of parameters in the total cross section curves on the left-hand side. The differences in the slopes are due to the different scales while the normalization difference is due to the choice of charm mass and the parton densities — the MRST densities generally give a larger cross section due to their larger α_s. However, the curves need to be scaled up by a factor of four to agree with the STAR normalization [4], as may be expected from the total cross section results.

To illustrate the effect of Peterson fragmentation, the p_T distribution with $\epsilon_c = 0.06$ in Eq. (3), is shown by the dot-dashed histogram in Fig. 1. The MRST parton densities are employed, along with $m = 1.2$ GeV, $\mu = 2m$, as in the solid curve. At $p_T \sim 10$ GeV, there is about a factor of 5 between the solid curve and the dot-dashed histogram while there is a slight increase for $p_T \leq 2$ GeV. If ϵ_c is decreased by a factor of 10, making it more consistent with the Mellin space result [24], the resulting dotted histogram is rather similar to the charm quark distribution in the solid curve. A similarly hard fragmentation function is used in the FONLL formalism, discussed in Frixione's talk [22], which matches fixed-order NLO terms to next-to-leading log, large p_T resummation to produce an improved result for $p_T \gg m$ [25].

The shape of the charm quark p_T distribution at $\sqrt{S} =$ 1.96 TeV also agrees quite well with the CDF data from the Tevatron [17]. Given the large discrepancy between the pQCD result and the STAR cross section, it might be surprising that the normalization is also in good agreement with the sum of the charged and neutral D data scaled to include D_s and Λ_c production. No total cross section is available because only charm hadrons with $p_T > 5$ GeV have been measured so far.

Factorization breaking for charm fragmentation has been suggested from studies of the x_F distributions of *e.g.* D^+ and D^- production, particularly in $\pi^- A$ interactions where the D^- is leading relative to the D^+ since the D^- shares a valence quark with the π^- while the D^+ does not. Several mechanisms such as intrinsic charm [18] and string drag have been proposed, both of which involve charm quark coalescence with spectators. Such comoving partons are naturally produced in a hard scattering. Although it is not intuitive to expect coalescence to work at high p_T, it seems to do so for charm. See the talks by Hwa [26] and Rapp [6] for discussions of coalescence models for light hadrons and charm.

3 Hidden Charm

We now turn to J/ψ production in dA interactions at RHIC and the LHC. It is essential that the A depen-

dence be understood in cold nuclear matter to set a proper baseline for quarkonium suppression in AA collisions. The NA50 collaboration [1,27] has studied the J/ψ A dependence and attributed its behavior to J/ψ break up by nucleons in the final state, referred to as nuclear absorption. However, the parton distributions are modified in the nucleus relative to free protons. This modification, referred to here as shadowing, is increasingly important at higher energies, as emphasized in Ref. [28]. In this section, we discuss the interplay of shadowing and absorption in d+Au collisions at RHIC and in d+Pb collisions at the LHC. Previously, we calculated the effect of shadowing alone on the J/ψ dA/pp ratio as a function of rapidity and impact parameter [28]. The large $c\overline{c}$ total cross section also has implications for the J/ψ yield if J/ψ's arise from $c\overline{c}$ recombination in a QGP [7]. Such a total cross section would suggest significant secondary J/ψ production at RHIC, leading to enhancement rather than suppression in central collisions. There is no evidence for a strong regeneration effect in the PHENIX Au+Au data so far [29].

Shadowing, the modification of the parton densities in the nucleus with respect to the free nucleon, may be taken into account by replacing f_j^p in Eq. (1) by $F_j^A(x,\mu^2,\boldsymbol{b},z) = \rho_A(\boldsymbol{b},z)S^j(A,x,\mu^2,\boldsymbol{b},z)f_j^p(x,\mu^2)$ and adding integrals over the spatial coordinates. Here S^j is the shadowing parameterization. The density distribution of the deuteron is also included in these calculations but the small effects of shadowing in deuterium is ignored. We did not discuss the effect of shadowing on the charm p_T distributions because the effect at midrapidity is small and, on the logarithmic scale of the p_T distributions, negligible. The J/ψ is another story due to the PHENIX muon capability at forward and backward rapidity. As shown in Leitch's talk [30], although the PHENIX J/ψ data are consistent with shadowing alone, the data are also consistent with nuclear shadowing plus a small absorption cross section of 1-3 mb, smaller than that currently obtained in SPS measurements [27]. We have calculated J/ψ production in the color evaporation model (CEM) using the same mass and scale as in $c\overline{c}$ production but cutting off the invariant mass of the pair at $4m_D^2$. The calculations of the dA/pp ratios are done at LO to simplify the calculations. As shown in Fig. 2, the LO and NLO ratios are equivalent. We have now also implemented nucleon absorption in the calculation, showing the effect of several absorption and production mechanisms.

To implement nuclear absorption on J/ψ production in dA collisions, the dN production cross section is weighted by the survival probability, $S^{\rm abs}$ [31]

$$S^{\rm abs}(\boldsymbol{b},z) = \exp\left\{-\int_z^\infty dz'\rho_A(\boldsymbol{b},z')\sigma_{\rm abs}(z'-z)\right\} \quad (4)$$

where z is the longitudinal production point and z' is the point at which the state is absorbed. The nucleon absorption cross section, $\sigma_{\rm abs}$, typically depends on where the state is produced in the medium and how far it travels through nuclear matter. If absorption alone is active, *i.e.* $S^j \equiv 1$, then an effective minimum bias A dependence is obtained after integrating $S^{\rm abs}$ over the spatial coordinates. If $S^{\rm abs} = 1$ also, $\sigma_{{\rm d}A} = 2A\sigma_{pN}$. When $S^{\rm abs} \neq 1$,

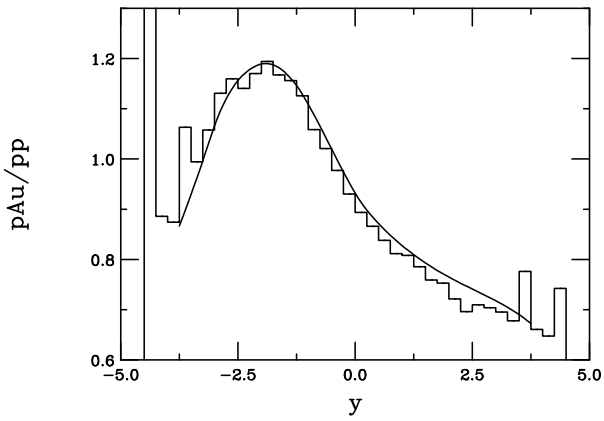

Fig. 2. The J/ψ pAu$/pp$ ratio at 200 GeV. We compare the NLO (solid histogram, MRST HO) and LO (solid curve, MRST LO) results using $m = \mu/2 = 1.2$ GeV with the EKS98 parameterization.

$\sigma_{{\rm d}A} = 2A^\alpha\sigma_{pN}$ where, if $\sigma_{\rm abs}$ is a constant, independent of the production mechanism for a nucleus of $\rho_A = \rho_0\theta(R_A - b)$, $\alpha = 1 - 9\sigma_{\rm abs}/(16\pi r_0^2)$, where $r_0 = 1.2$ fm. The contribution to the full A dependence in $\alpha(x_F)$ from absorption alone is only constant if $\sigma_{\rm abs}$ is constant and independent of the production mechanism [31]. The observed J/ψ yield includes feed down from χ_{cJ} and ψ' decays, giving

$$S^{\rm abs}_{J/\psi}(b,z) = 0.58S^{\rm abs}_{J/\psi,\,{\rm dir}}(b,z) + 0.3S^{\rm abs}_{\chi_{cJ}}(b,z) + 0.12S^{\rm abs}_{\psi'}(b,z)\ . \quad (5)$$

The J/ψ may be produced as a color singlet, a color octet or in a combination of the two. In color singlet production, the final state absorption cross section depends on the size of the $c\overline{c}$ pair as it traverses the nucleus, allowing absorption to be effective only while the cross section is growing toward its asymptotic size inside the target. On the other hand, if the $c\overline{c}$ is only produced as a color octet, hadronization will occur only after the pair has traversed the target except at very backward rapidity. We have considered a constant octet cross section, as well as one that reverts to a color singlet at backward rapidities. For singlets, $S^{\rm abs}_{J/\psi,\,{\rm dir}} \neq S^{\rm abs}_{\chi_{cJ}} \neq S^{\rm abs}_{\psi'}$ but, with octets, one assumes that $S^{\rm abs}_{J/\psi,\,{\rm dir}} = S^{\rm abs}_{\chi_{cJ}} = S^{\rm abs}_{\psi'}$. As can be seen in Fig. 3, the difference between the constant and growing octet assumptions is quite small at large $\sqrt{S_{NN}}$ with only a small singlet effect at $y < -2$ and -5 at RHIC and the LHC respectively. Singlet absorption is also important only at similar rapidities and is otherwise not different from shadowing alone. Finally, we have also considered a combination of octet and singlet absorption in the context of the NRQCD approach, see Ref. [31] for more details. The combination of nonperturbative singlet and octet parameters changes the shape of the shadowing ratio slightly. Including the singlet contribution weakens the effective absorption. The results are shown integrated over impact parameter. The calculations use the EKS98 shadowing parameterization [32] since it gives good agreement

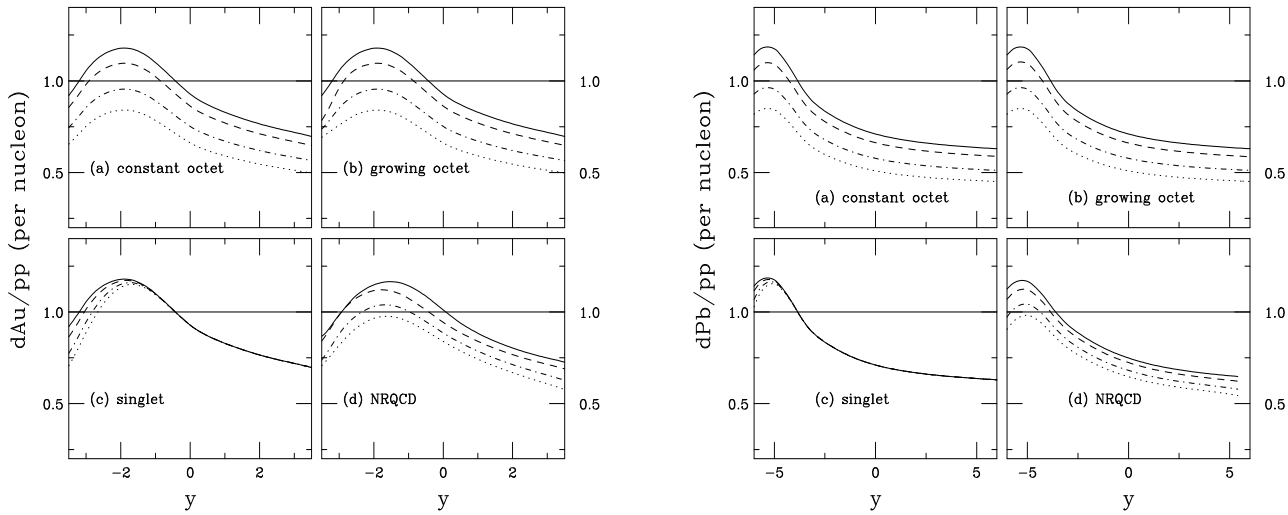

Fig. 3. The J/ψ dA/pp ratios with EKS98 for $\sqrt{S_{NN}} = 200$ GeV (left-hand side) and for $\sqrt{S_{NN}} = 6.2$ TeV (right-hand side) as a function of the J/ψ rapidity for (a) constant octet, (b) growing octet, (c) singlet, all calculated in the CEM and (d) NRQCD. For (a)-(c), the curves are no absorption (solid), $\sigma_{\rm abs} = 1$ (dashed), 3 (dot-dashed) and 5 mb (dotted). For (d), we show no absorption (solid), 1 mb octet/1 mb singlet (dashed), 3 mb octet/3 mb singlet (dot-dashed), and 5 mb octet/3 mb singlet (dotted).

with the trend of the PHENIX data. For results with other shadowing parameterizations, see Ref. [33].

Several values of the asymptotic absorption cross section, $\sigma_{\rm abs} = 1$, 3 and 5 mb, corresponding to $\alpha = 0.98$, 0.95 and 0.92 respectively using Eqs. (4) and (5) are shown in Fig. 3. These values of $\sigma_{\rm abs}$ are somewhat smaller than those obtained for the sharp sphere approximation. The diffuse surface of a real nucleus and the longer range of the density distribution result in a smaller value of $\sigma_{\rm abs}$ than a spherical nucleus. There is good agreement with the trend of the preliminary PHENIX data [34] for $\sigma_{\rm abs} = 0-3$ mb. We use $\sigma_{\rm abs} = 3$ mb in our further calculations to illustrate the relative importance of absorption and shadowing.

We now turn to the centrality dependence of J/ψ production in dA collisions. In central collisions, inhomogeneous shadowing is stronger than the homogeneous result. The stronger the homogeneous shadowing, the larger the inhomogeneity. In peripheral collisions, inhomogeneous effects are weaker than the homogeneous results but some shadowing is still present. Shadowing persists in part because the density in a heavy nucleus is large and approximately constant except close to the surface and because the deuteron wave function has a long tail. We also expect absorption to be stronger in central collisions.

To study the centrality dependence of shadowing and absorption, we present the dA/pp ratios as a function of the number of binary NN collisions, $N_{\rm coll}$,

$$N_{\rm coll}(b) = \sigma_{NN}^{\rm in} \int d^2s T_A(s) T_B(|\boldsymbol{b} - \boldsymbol{s}|)$$

where T_A and T_B are the nuclear thickness functions and $\sigma_{NN}^{\rm in}$ is the inelastic nucleon-nucleon cross section, 42 mb at 200 GeV and 76 mb at 6.2 TeV. In Fig. 4, we show the $N_{\rm coll}$ dependence for several representative rapidities, $y = -2$, 0 and 2 for RHIC (left-hand side) and $y = -4$, -2, 0, 2 and 4 for the LHC (right-hand side). We have chosen an inhomogeneous shadowing parameterization proportional to the path length of the parton through the nucleus [28]. For results with other parameterizations, see Ref. [33].

The dependence of the RHIC ratios on $N_{\rm coll}$ is almost linear, as seen on the left-hand side of Fig. 4. We do not show results for $N_{\rm coll} < 1$. The weakest $N_{\rm coll}$ dependence occurs in the antishadowing region, illustrated by the $y = -2$ result (dot-dashed curve). The trends of the ratios as a function of $N_{\rm coll}$ are consistent with the PHENIX data from the north muon arm ($y = 2$) and the electron arms ($y = 0$) but the preliminary PHENIX results from the south arm ($y = -2$) are much stronger than our predictions and, in fact, go the opposite way [30]. The overall dependence on $N_{\rm coll}$ is stronger than that obtained from shadowing alone, described in Ref. [28] where inhomogeneous shadowing effects depend strongly on the amount of homogeneous shadowing. Relatively large effects at low x are accompanied by the strongest b dependence. In the transition region around midrapidity at RHIC, the b dependence of the ratio dAu/pp due to shadowing is nearly negligible and almost all the $N_{\rm coll}$ dependence at $y \sim 0$ can be attributed to absorption. The $y = -2$ results for color singlet production and absorption, in the antishadowing region, are fairly independent of $N_{\rm coll}$.

On the right-hand side of Fig. 4 we present our inhomogeneous shadowing and absorption calculations for d+Pb collisions at $\sqrt{S_{NN}} = 6.2$ TeV at the LHC. Results for $y = \pm 4$, in the range of the ALICE muon arm, are also included. Given that the rapidity range of the muon arm encompasses the crossover point where dPb/$pp \sim 1$ at $y \sim -3.9$, the centrality dependence of absorption alone could be determined and used to calibrate the inhomogeneous shadowing effects. Note that is is only possible to reach $y \sim -3.9$ in ALICE by running Pb+d since the

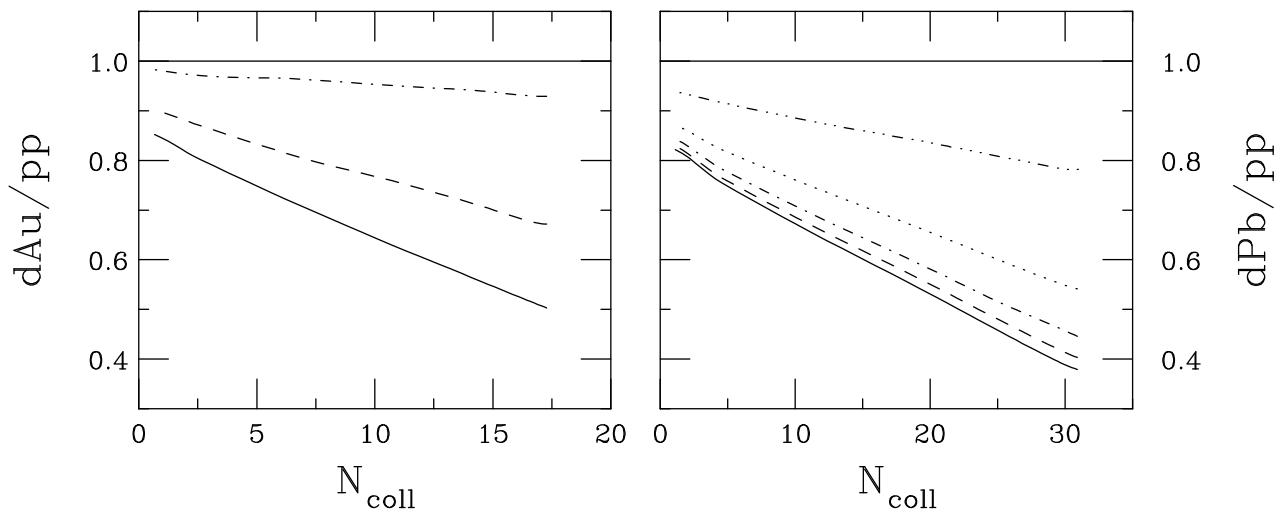

Fig. 4. The dA/pp ratio as a function of $N_{\rm coll}$ for a growing octet with $\sigma_{\rm abs} = 3$ mb and the EKS98 parameterization. Left-hand side: results for $y = -2$ (dot-dashed), $y = 0$ (dashed) and $y = 2$ (solid) at 200 GeV. Right-hand side: results for $y = -4$ (dot-dot-dot-dashed), $y = -2$ (dotted), $y = 0$ (dot-dashed), $y = 2$ (dashed) and $y = 4$ (solid) at 6.2 TeV.

muon arm is only on one side of midrapidity. Both ALICE and CMS should be able to measure J/ψ production at $y = \pm 2$ and 0. The results for $y = 4$, ± 2 and 0, all in the low x shadowing region, are rather closely grouped together. This should not be surprising because the EKS98 shadowing ratios shown on the right-hand side of Fig. 3 are not very strong functions of rapidity. Note that the x-axis scale is expanded relative to that of RHIC due to the larger $\sigma_{NN}^{\rm in}$ at 6.2 TeV.

4 Summary

In conclusion, the RHIC d+Au data on open charm and J/ψ are beginning to come into their own. While the QCD calculations agree well with the shape of the STAR p_T distributions, they underestimate the reported total cross section. In contrast, the J/ψ cross section is in relatively good agreement with QCD predictions and the agreement of the minimum bias data with calculations including shadowing and nucleon absorption is quite good. The agreement of the J/ψ calculations with the preliminary PHENIX data is generally quite good, except for the dependence of the $y \approx -2$ results on $N_{\rm coll}$.

References

1. L. Kluberg, these proceedings.
2. K. Adcox *et al.* (PHENIX Collaboration), Phys. Rev. Lett. **88**, (2002) 192303.
3. A.P. Suaide, these proceedings.
4. M. Calderon, these proceedings.
5. M. Djordjevic, these proceedings.
6. R. Rapp, these proceedings.
7. R.L. Thews, these proceedings.
8. O. Drapier, these proceedings.
9. S. Frixione, M.L. Mangano, P. Nason and G. Ridolfi, Adv. Ser. Direct High Energy Phys. **15**, (1998) 609.
10. P. Nason, S. Dawson and R.K. Ellis, Nucl. Phys. B **303**, (1988) 607.
11. N. Kidonakis, E. Laenen, S. Moch, and R. Vogt, Phys. Rev. D **67**, (2003) 074037.
12. N. Kidonakis and R. Vogt, Eur. J. Phys. C **36**, (2004) 201.
13. R. Vogt, Heavy Ion Phys. **17**, 75 (2003)
14. P.L. McGaughey *et al.* Int. J. Mod. Phys. A **10**, (1995) 2999; R. Vogt, Int. J. Mod. Phys. E **12**, (2003) 211.
15. J. Adams *et al.* (STAR Collaboration), nucl-ex/0407006.
16. O. Botner *et al.* (UA1 Collaboration) Phys. Lett. B **236**, (1990) 488.
17. D. Acosta *et al.* (CDF II Collaboration) Phys. Rev. Lett. **91**, (2004) 241804.
18. R. Vogt, S.J. Brodsky and P. Hoyer, Nucl. Phys. B **383**, (1992) 643.
19. C. Peterson, D. Schlatter, I. Schmitt, and P. Zerwas, Phys. Rev. D **27**, (1983) 105.
20. J. Chirn, Z. Phys. C **36**, (1987) 163.
21. K. Abe *et al.* (BELLE Collaboration), BELLE-CONF-0335 (2003).
22. S. Frixione, these proceedings.
23. M. L. Mangano, P. Nason and G. Ridolfi, Nucl. Phys. B **405**, (1993) 507.
24. S. Frixione, private communication.
25. M. Cacciari, P. Nason and R. Vogt, hep-ph/0502203.
26. R. Hwa, these proceedings.
27. G. Borges, these proceedings.
28. S.R. Klein and R. Vogt, Phys. Rev. Lett. **91**, 142301 (2003).
29. M. Rosati, these proceedings.
30. M. Leitch, these proceedings.
31. R. Vogt, Nucl. Phys. A **700**, 539 (2002).
32. K.J. Eskola, V.J. Kolhinen and P.V. Ruuskanen, Nucl. Phys. B **535**, (1998) 351; K.J. Eskola, V.J. Kolhinen and C.A. Salgado, Eur. Phys. J. C **9**, (1999) 61.
33. R. Vogt, Phys. Rev. C, in press, hep-ph/0411378.
34. R. de Cassagnac (PHENIX Collaboration), J. Phys. G **30**, (2004) S1341.